A Nanobody as a Potent Angiogenesis Inhibitor That Targets the Orphan Receptor Tie1

May Meltzer
Ben-Gurion University of the Negev
Noam Eliash
Ben-Gurion University of the Negev
Niv Papo (papo@bgu.ac.il)
Ben-Gurion University of the Negev https://orcid.org/0000-0002-7056-2418

Research Article

Keywords: Nanobody, protein engineering, receptor tyrosine kinase, angiogenesis, cell migration

Posted Date: February 15th, 2022

DOI: https://doi.org/10.21203/rs.3.rs-1330228/v1

Abstract

Human Tie1 and Tie2 receptor tyrosine kinases (RTKs) are signaling molecules with important pathophysiological functions in many diseases, including different cancers. Tie1, in particular, has been implicated in the promotion of tumor growth and cancer cell migration *in vitro* and *in vivo*. Tie1 activity is mediated mainly through the downstream angiopoietin-1 (Ang1)-dependent activation of Tie2, rendering both Tie 1 and the Tie1/Tie2/Ang1 axis attractive putative targets for therapeutic intervention. However, the development of inhibitors that target Tie1 and their effect on Tie2 or on the Tie1/Tie2/Ang1 axis in general remains an unfulfilled task, due, largely, to the facts that Tie1 is an orphan receptor and is difficult to produce and use in the quantities required for immune antibody library screens. In a search for a selective inhibitor of this orphan receptor, we sought to exploit the advantages (e.g., small size that allows them to bind to hidden epitopes) of non-immune nanobodies and to simultaneously overcome their limitations (i.e., low expression and stability). We thus performed expression, stability and affinity screens of yeast-surface-displayed naïve and predesigned synthetic (non-immune) nanobody libraries against the Tie1 extracellular domain. The screens yielded a nanobody with high expression and good affinity and specificity for Tie1, thereby yielding preferential binding for Tie 1 over Tie2. The stability, selectivity, potency, and therapeutic potential of this synthetic nanobody were profiled using *in vitro* and cell-based assays. The nanobody triggered a Tie1-dependent inhibition of RTK (Tie2, Akt and FAK) phosphorylation and angiogenesis in endothelial cells, and suppression of cancer cell proliferation and migration.

Introduction

Orphan receptors, i.e., receptors whose natural ligands and biological functions are yet to be elucidated, present challenging targets for drug discovery, as they appear to be associated with a variety of diseases, but the particular diseases, like the ligands, remain elusive. The current 'lack' of a natural ligand for the orphan receptor, Tie1 receptor tyrosine kinase (RTK), is undoubtedly complicating research on its function (1). It is, however, known that Tie1 and its family member Tie2, which are expressed in endothelial cells (2, 3), are key regulators of normal blood and lymphatic vessel development and also of pathological processes, including tumor angiogenesis, progression and metastasis, atherosclerosis, and vascular leakage (4, 5). More specifically, it is known that Tie1, together with Tie2 and its natural ligand angiopoietin-1 (Ang1), are essential for normal blood vessel maturation (6–8), and that the expression of Tie1 is increased in tissue angiogenesis and cancerous processes. Conversely, deletion of Tie1, and also of Tie2, results in reduced angiogenesis and tumor growth (5, 9–11). Importantly, it is also known that when Tie1 located on the endothelial cell membrane complexes with the Tie2-Ang1 receptor-ligand pair, the complex becomes concentrated at the cell-cell contact interface (12–14), where Ang1 activates (although does not bind directly to) Tie1 (5, 12, 15). Similarly, it has been shown *in vivo* in mouse endothelial cells that Tie1 deletion reduces Ang1-induced phosphorylation of Tie2, indicating that Tie1 affects the process of Ang1-induced Tie2 activation and the downstream focal adhesion kinase (FAK)/phosphoinositide 3-kinase (PI3K)/protein kinase B (Akt) signaling pathway that leads to tumor growth and vascularization (9, 16).

While the Ang1-Tie2 axis has been well researched, especially with regard to endothelial and cancer cell sprouting, migration, and survival (17–19), the signaling pathways and cellular functions regulated specifically by Tie1 have been less well studied, primarily due to the lack of suitable biochemical tools. The lack of progress in research on Tie1 would appear to be somewhat surprising in light of the close homology exhibited by Tie1 and Tie2 (5), with the amino acid sequences of their cytoplasmic kinase domains showing about 80% identity [although their extracellular domains are more diverse, with different studies reporting their identity to be 24–59% (20–23)]. Efforts are thus underway to pinpoint natural proteins and protein variants that specifically target the extracellular domain of Tie1. For example, in liver tissue, the secretory protein, leukocyte cell-derived chemotaxin 2 (LECT2), was shown to bind to Tie1, resulting in dephosphorylation of Tie1 and the consequent disruption of Tie1-Tie2 interactions, which eventually led to enhanced liver fibrosis (24). In contrast, COMP-Ang1, a synthetic recombinant Ang1 multimeric variant, was shown to stimulate Tie1 phosphorylation in endothelial cells (12, 25).

A possible way forward to revealing the signaling pathways and cellular functions regulated by Tie1 was thought to lie in the development of targeting antibodies; for example, a Tie1-targeted function-blocking antibody, designated AB-Tie1-39, was found to inhibit Tie1 and thereby to lead to a decrease in Tie2-mediated Akt phosphorylation (26). This research approach was, however, impeded by the well-known limitations of antibodies (despite their significant clinical success), including: their inability to site specifically incorporate chemical modalities, their potential undesired effector functions (27, 28), the high cost of their recombinant production in mammalian cells (28) and the considerable intellectual property barriers to their development (29). An answer to these limitations may lie in nanobodies, single-domain antibodies obtained from camelids (llamas, camels, alpacas, or their relatives) (30). The inherent advantages of nanobodies include their small size (~ 15 kDa, 4 nm long and 2.5 nm wide), their high solubility, stability, specificity, affinity, and thermal and chemical resistance, and the ease of cloning them. In addition, nanobodies have a low immunogenic profile, which makes them suitable for human use. Among the above properties of nanobodies, their small size is particularly important, because it facilitates their use for targeting antigens with small or inaccessible binding pockets (31). The interaction of nanobodies with such antigens is facilitated by the three complementarity-determining regions (CDRs) CDR1–3 and their attendant framework residues. Of note, CDR3 is the main contributor to antigen specificity, whereas CDR1 and CDR2 are responsible for binding strength (32, 33).

In research and in therapeutic applications, nanobodies can be used either as antagonists (i.e., to compete for binding of effector molecules) or to create conformational (e.g., allosteric) changes in their target receptors that prevent their recognition by their natural ligands (31). Therefore, the use of nanobodies rather than classical antibodies may provide the means to overcome some of the current challenges in the development of drugs targeting orphan receptors. However, current methods for generating nanobody-based compounds remain slow, expensive, and often unreliable. These problems derive primarily from the method of nanobody preparation, which includes the drawn-out and costly step of immunization of a camelid. To address these problems and to open the way for nanobody development, previous efforts have combined yeast (or phage) display affinity screens with synthetic (non-immune) libraries (34). However, it still remains particularly challenging to identify, in synthetic

libraries, nanobodies that exhibit the desired combination of stability and high expression (35, 36). It is against this background that we sought to develop both a nanobody that would bind strongly to Tie1 and a protocol for the inexpensive and facile production of such a nanobody. Our protocol was based on randomly mutating the CDR regions of a predesigned synthetic nanobody library [previously devised using an alignment of structurally characterized nanobodies from the Protein Data Bank (PDB)] and then screening the library by using a cell-based selection scheme enabled by fluorescence activated cell sorting (FACS). The methodology enabled us to identify a stable nanobody that binds strongly to Tie1 and will also bind to Tie2 but less preferentially than to Tie1. This nanobody, which we designated NB19, was found to bind the recombinant human Tie1 extracellular domain, designated here as Tie1-ECD, with a K_D in the subnanomolar range and, importantly, to show selectivity for Tie1 over Tie2 *in vitro* and in cells. We also showed that NB19 significantly inhibits Tie1 and Tie2 phosphorylation in a dose-dependent manner and thus acts as functional antagonist of Tie1, leading to reduced angiogenesis and inhibition of cancer proliferation and migration. By exploiting the ability of NB19 to bind both Tie1 and Tie2, but with preference for Tie1, we were able to explore and dissect out the specific roles of each of these two receptors in angiogenesis and cancer growth and migration.

Materials And Methods

Generation and purification of the anti-Tie1 nanobody

The protocol for nanobody generation was adapted from Shlamkovich et al. (37). The selected nanobody (i.e., NB19) was purified using periplasmic extraction, followed by Ni-NTA affinity chromatography and size-exclusion chromatography (SEC), as described in detail in the supplementary information (SI) section.

NB19 binding analysis using surface plasmon resonance (SPR)

The binding interactions between NB19 and Tie1-ECD were analyzed (Proteomics Unit, NIBN, BGU) in real time by surface plasmon resonance (SPR) on a ProteOn XPR36 instrument (Bio-Rad, Hercules, CA, USA). The ProteOn GLC sensor chip was initialized in air, and PBST (PBS, 0.005% Tween) buffer was flushed through the instrument prior to the binding experiments. The purified NB19 protein was immobilized on the surface of the GLC sensor chip by using the amine coupling reagents N-hydroxysuccinimide (0.1 M; sulfo-NHS) and 1-ethyl-3-(3-dimethylaminopropyl)-carbodiimide (0.4 M; EDC; Bio-Rad), as follows. NB19 (10 µg) in 10 mM sodium acetate, pH 4.0, was allowed to flow over an activated GLC sensor chip channel surface, at a flow rate of 30 µL/min, until the target immobilization level was reached. Bovine serum albumin (BSA), 3 µg, in 10 mM sodium acetate, pH 4.5, was then allowed to flow over the activated surface of a control GLC sensor chip channel at a flow rate of 30 µL/min until the NB19 ligand immobilization level was reached. After NB19 immobilization, the chip surface was treated with 1 M ethanolamine HCl at pH 8.5 to deactivate excess reactive esters. All binding experiments were performed at 25°C in a degassed binding buffer (PBS, pH 7.4). Recombinant human Tie1-ECD (R&D Systems, Minneapolis, MN, USA) and recombinant human Tie2 extracellular domain (Tie2-ECD, R&D Systems) at a range of concentrations (10–0.625 nM and 50–6.25 nM, respectively) were allowed to flow over the

surface-immobilized NB19 at a flow rate of 30 µL/min for 60 min, and the Tie1-ECD–NB19 and Tie2-ECD–NB19 binding interactions were monitored. After complex dissociation, which was monitored for 60 min, a regeneration step with 50 mM NaOH at a flow rate of 100 µL/min was performed. The analyte sensorgram run was normalized by subtracting the BSA-immobilized channel and the zero-analyte concentration runs. The binding constant (K_D) was determined from the sensorgrams of the equilibrium binding phase. Binding kinetics of NB19 were analyzed by fitting to a Langmuir model.

Cell culture

Human embryonic kidney 293 cells (HEK293; ATCC, Manassas, VA, USA) were cultured in complete growth medium composed of DMEM High Glucose (Biological Industries, Kibbutz Beit-Haemek, Israel) supplemented with 10% fetal bovine serum (FBS) (Thermo Fisher Scientific, Waltham, MA, USA), 1% l-glutamine (Biological Industries), and 1% penicillin/streptomycin (Biological Industries) under 5% CO_2 at 37°C. HEK293 cells, which lack endogenous Tie receptors, were transiently transfected with full-length HA-tagged Tie1 (pCMV3-TIE1-HA refseq: NM_005424.2) and full-length myc-tagged Tie2 (pCMV3-C-Myc redseq: NM_000459.3). When the cells reached 80–90% confluence in 6-well plates, transfections were performed using Lipofectamine 2000 (Invitrogen, USA) according to the manufacturer's instructions. Human telomerase-immortalized microvascular endothelium (TIME) cells (ATCC), which endogenously express Tie1 and Tie2, were cultured under 5% CO_2 at 37°C, in Vascular Cell Basal Medium (ATCC) supplemented with 10% FBS and Microvascular Endothelial Cell Growth Kit-VEGF (ATCC) according to the manufacturer's instructions. Human glioblastoma (U87-MG) cells were grown under 5% CO_2 at 37°C in minimum essential medium supplemented with 10% FBS, 1% l-glutamine, and 1% penicillin/streptomycin.

Cell-binding assay using flow cytometry

Expression of Tie1 and Tie2 and binding of purified NB19 to receptor-expressing cells was analyzed by flow cytometry using TIME or U87-MG cells endogenously expressing Tie1 and Tie2 and HEK293 cells overexpressing Tie1, Tie2 or both receptors. To determine the expression levels of Tie1 and Tie2 in HEK293 cells following transient transfection, cells were centrifuged and resuspended in 100 µL of PBSA with 1:100 allophycocyanin (APC)-labeled anti-human Tie2 antibody (BioLegend) or phycoerythrin (PE)-labeled anti-human Tie1 antibody (R&D Systems), incubated at 4°C for 30 min, and washed three times with 100 µL of PBSA before flow cytometry analysis. Unstained cells were used to determine the background signal. For binding assays, Tie1- and Tie2-expressing TIME (or U87-MG) cells and HEK293 cells transiently transfected with Tie1, Tie2 or both receptors were incubated with NB19 at different concentrations in a total volume of 200 µL of PBSA at 4°C for 1 h with gentle agitation. Thereafter, the cell suspensions were centrifuged at 150 g at 4°C for 5 min and washed three times with 100 µL of PBSA. Cells were then resuspended in 100 µL of PBSA containing a 1:200 dilution of APC-conjugated anti-FLAG antibody (BioLegend) for the detection of NB19 bound to the cells. After 30 min on ice, the cells were washed twice in PBSA and analyzed by flow cytometry with a BD FACSCanto™ II Flow Cytometry System (BD Biosciences, San Jose, CA, USA). Mean fluorescence levels of the background were subtracted, and the data was analyzed using FlowJo (Tree Star Inc., OR, USA) analysis software.

Immunofluorescence microscopy

HEK293 cells were seeded on sterile cover slips and grown to confluence before being transfected using Lipofectamine 2000 (Invitrogen) with plasmids encoding either full-length HA-tagged Tie1 (pCMV3-TIE1-HA; refseq: NM_005424.2) or full-length myc-tagged Tie2 (pCMV3-C-Myc; redseq: NM_000459.3). Untransfected cells were used as the negative control. Twenty-four hours post-transfection, the cells were washed with PBS and then incubated for 30 min at 4°C with 100 nM NB19. The cells were then washed with PBS, fixed for 15 min in 4% paraformaldehyde, and permeabilized for 10 min with 0.5% Triton X-100)Bio-Lab Ltd, Jerusalem, Israel) in PBS. The cells were blocked for 30 min with gentle shaking at room temperature in 5% BSA in PBS, followed by two washes with PBS. The cells were then incubated in 5% BSA/PBS for 1 h at 4°C with FITC anti-human Tie2 (BioLegend) or PE-labeled anti-human Tie1 (BioLegend), and APC-conjugated anti-FLAG antibody (BioLegend) for the detection of NB19 colocalization with Tie1 and Tie2. Confocal images were captured using a 20× Zeiss Plan-Apochromat dry, 0.8 NA, DIC objective on a laser scanning confocal microscope (Zeiss Axio-Observer Z1 inverted microscope, Ilse Katz Institute for Nanoscale Science & Technology, BGU) and analyzed with Zeiss software.

Inhibition of Tie1 by siRNA

For small interfering RNA (siRNA)-mediated knockdown of Tie1, TIME cells were plated at 80% confluency one day before transfection and then transfected with Tie1 siRNA using the TriFECTa RNAi kit (IDT, San-Jose, CA) with the Lipofectamine 3000 reagent (Invitrogen) according to the manufacturer's instructions.

Tie1, Tie2, Akt and FAK phosphorylation assays

Confluent TIME cells were cultured on 12-well plates in growth-factor depleted Vascular Cell Basal Medium (ATCC) supplemented with 0.5% FBS for 12 h at 37°C, under 5% CO_2. The cells were then washed with PBS, and the medium was exchanged with fresh Vascular Cell Basal Medium depleted of growth factors and serum (ATCC). Following treatment with 1 mM sodium orthovanadate (Na_3VO_4; Sigma) for 15 min, the cells were co-incubated for 15 min (for Tie1 and Tie2 analysis), or for 30 min (for FAK and Akt analysis), at 37°C with either 500 ng/ml human recombinant Ang1 (R&D systems) as the positive control, or 30 nM (or 300 nM) NB19 combined with 500 ng/ml Ang1. Non-stimulated (in the absence of Ang1) cells served as the negative control. The cells were then washed twice with PBS containing 1 mM Na_3VO_4 and lysed in ice-cold lysis buffer [20 mM HEPES, pH 7.4, 150 mM NaCl, 1% TritonX-100, 1 mM Na_3VO_4, and 1× complete protease inhibitor cocktail tablet (Roche, USA)]. The cells were scraped from the culture plate wells, and the lysates were clarified by centrifugation (13,000 rpm for 30 min at 4°C). Protein concentration was measured by the bicinchoninic acid (BCA) assay (Thermo Fisher Scientific), and equivalent amounts of each lysate sample were analyzed by 10% SDS-PAGE transferred to PVDF blotting membranes (BioRad). Blots were blocked (5% BSA, 50 mM Tris-HCl, pH 7.4, 150 mM NaCl, 0.1% Tween 20) for 1 h at room temperature and then probed, following an overnight incubation at 4°C, with the following antibodies, all at a 1:1000 dilution: phospho-Tie1 (Tyr1117) specific rabbit polyclonal antibody

(Invitrogen), anti-Tie1-specific rabbit monoclonal antibody (Cell Signaling Technology, Danvers, MA, USA), phospho-Tie2 (Y992) specific rabbit polyclonal antibody (R&D Systems), anti-Tie2-specific rabbit monoclonal antibody (Cell Signaling Technology), anti-phospho-Akt-specific antibody (Cell Signaling Technology), anti-Akt-specific antibody (Cell Signaling Technology), anti-phospho-FAK-specific (Tyr397) antibody (Cell Signaling Technology) or anti-FAK-specific antibody (Cell Signaling Technology). PVDF membranes were washed three times with TBST (50 mM Tris-HCl, pH 7.4, 150 mM NaCl, 0.1% Tween 20) and probed with a 1:1000 dilution of HRP-linked anti-rabbit antibodies (Cell Signaling Technology) for 1 h at room temperature. Membranes were washed three times with TBST and then visualized and quantified using chemiluminescence (ECL, Biological Industries) and ImageJ software, respectively. The intensities of the phospho-Tie1, phospho-Tie2, phospho-Akt, and phospho-FAK bands were adjusted for the expression of total Tie1, Tie2, Akt, and FAK, respectively, for each experiment. Blots were stripped and re-probed with a 1:1000 dilution of anti-β-actin antibody (Cell Signaling Technology) followed by an HRP-conjugated anti-mouse antibody (at 1:1000 dilution, Cell Signaling Technology) for further normalization. Each experimental condition was repeated in triplicate. Band intensities of the phosphorylated proteins (Tie1, Tie2, Akt, and FAK) (as measured by ImageJ software) were normalized to the respective total protein levels, and this value was subsequently normalized to the total amount of β-actin for each sample.

Capillary-like tube formation assay

Serum-reduced Matrigel (10 mg/ml; BD Biosciences) was thawed overnight at 4°C, and 150 µL were added to each well of a µ-Slide 8 Well (ibidi, Gräfelfing, Germany) and allowed to solidify for 1 h at 37°C. In each well, the Matrigel was then incubated with 1×10^5 TIME cells treated with either 500 ng/mL Ang1 or with a combination of 500 ng/mL Ang1 and 30 nM (or 300 nM) NB19; untreated cells were used as the negative control. The cells were incubated for 18 h at 37°C, under 5% CO_2, and then washed twice in Hanks' balanced salt solution (Sigma-Aldrich). Capillary tube formation was observed on confocal images captured using a the Zeiss Plan-Apochromat laser scanning confocal microscope described above and analyzed with Zeiss software. Tube structures were analyzed for the number of junctions generated, and the total tube length was quantified by the analysis of digitized images of the capillary-like structures using ImageJ software and the Angiogenesis Analyzer plugin.

Cell proliferation assay

The effects of NB19 on the growth and survival of TIME or U87-MG cells were assessed by an XTT assay (2,3-bis [2-methoxy-4-nitro-5-sulfophenyl]-*2H*-tetrazolium-5-carboxanilide inner salt assay; Biological Industries). TIME or U87-MG cells were seeded (7,500 cells per well) on a human vitronectin-coated 96-well microplate (R&D systems) and incubated in growth medium for 24 h at 37°C, under 5% CO_2. The cell growth medium was then replaced with fresh Vascular Cell Basal Medium (ATCC) or minimum essential medium for TIME or U87-MG cells, respectively. In each case the medium was supplemented with 2% FBS and growth factor supplements, and the cells were incubated with either 500 ng/mL Ang1 or with a combination of 500 ng/mL Ang1 and 30 nM (or 300 nM) NB19 for 24 h at 37°C, under 5% CO_2. Viable

cells from each condition were measured by XTT at UV 450 nm, as described in the manufacturer's protocol. The UV readings of the cell-only (untreated) control were set at 100% viability, and readings from cells treated with NB19, a mixture of NB19 and Ang1, or Ang1 alone were expressed as % of the control.

Wound healing assay

The *in-vitro* wound healing assay was performed as previously described with some modifications (38). Briefly, U87-MG cells were seeded in 24-well plates at a density of 1.5×10^5 cells in each well and allowed to grow for 24 h at 37°C, under 5% CO_2, until they reached confluence. A linear scratch was created in each confluent monolayer by gently scraping the surface a with sterile p200 pipette tip (care was taken during scratching process to ensure similar scratches for all samples). The scratched monolayers were then washed twice to remove nonadherent cells. Ang1 (500 ng/mL)-treated cells were used as the positive control, and untreated cells, as the negative control. Test samples included mixtures of 30 nM (or 300 nM) of NB19 and Ang1 (500 ng/mL). Images were taken exactly at the same position prior to and post incubation of the cells with the different treatments or controls so as to document the wound closure process. Wounds were viewed under a light microscope immediately after the scratches were made and again after 6, 12, 18, and 24 h of incubation at 37°C in a 5% CO_2 incubator. The experiment was performed in triplicate, and the images were analyzed using ImageJ.

Statistical analysis

Data were analyzed with GraphPad Prism version 9.00 for Windows (La Jolla, CA). SD (standard deviation) was determined from at least three independent experiments. Comparisons between the groups were performed using a t-test (for two independent samples) and with one-way ANOVA (for multiple groups). A probability value of < 0.05 was considered statistically significant.

Results

Screening the Naïve NBlib library for nanobodies with a high affinity to Tie1-ECD

To produce highly expressed stable nanobodies exhibiting affinity to Tie1, three approaches were taken. In this – the first – approach, a synthetic (non-immune) naïve nanobody library, designated Naïve NBlib, was generated by randomizing (using NNS degenerate codons) specific positions within the three CDR loops (i.e., CDR1 at positions 25-34, CDR2 at positions 52-68, and CDR3 at positions 98-114) of a single nanobody clone that was previously isolated by the BGU group from a camel-derived nanobody library (39). This parental nanobody clone was shown to be highly stable, and its solved crystal structure enabled us to accurately identify CDR positions that were likely to tolerate mutagenesis with only a minimal effect on the structure and stability of the mutated nanobody (39). The Naïve NBlib library that was generated from four assembly PCRs of NNS-bearing DNA ultramer pairs was transformed into yeast, yielding 10^8 variants (Supplementary Fig. S1). The Naïve NBlib library was then sorted for high expression and increased affinity to Tie1-ECD by using seven consecutive rounds of affinity sorts, each one with a decreasing concentration of Tie1 (Supplementary Fig. S2). To identify high affinity nanobody

variants, 20 individual clones were randomly isolated from the seventh affinity sort. The level of binding to Tie1 of each of these 20 nanobody variants (normalized to their expression level) was then determined (Supplementary Fig. S3A). Sequencing analysis of the 10 variants that showed the highest affinity to Tie1 revealed unique sequences that were repeatedly identified in two variants (Supplementary Fig. S3B), namely, clone 7.16 with an apparent K_D of 12.81 nM and clone 7.20 with an apparent K_D of 15.72 nM [where the K_D values were estimated from titrations of clones 7.16 and 7.20 displayed on the yeast surface for affinity to soluble Tie1 (Supplementary Fig. S3C)]. Nevertheless, our attempts to produce these nanobody variants as soluble proteins were unsuccessful due to their lack of expression or low proteolytic stability in *Saccharomyces cerevisiae*.

Treating the Naïve NBlib library with trypsin or chymotrypsin before sorting produces proteolytically stable nanobody variants

To select nanobody clones likely to show high expression, proper folding, and stability (to both heat and proteolysis), our second approach comprised treating the parental Naïve NBlib library, prior to affinity screening, with a protease according to the protocol of Rocklin et al. (36). This methodology was chosen as a means to eliminate unfolded protein variants, which are particularly susceptible to cleavage (Supplementary Fig. S4A) (36). After treating Naïve NBlib libraries with trypsin (Supplementary Fig. S4B) or chymotrypsin (Supplementary Fig. S4C) at various concentrations, flow cytometry analysis of the treated library clones labeled with a mouse anti c-myc antibody, followed by an anti-mouse antibody conjugated to PE, was performed to detect expression levels (as an indication of the complete amino acid sequence and correct folding) (Supplementary Fig. S4B,C). The conditions giving the highest expression levels, namely, chymotrypsin as the protease and a concentration of 30 nM, were chosen for sorting the Naïve NBlib library to identify stable nanobodies. This treatment gave an expression level of the library of 10%, as shown in the red fluorescence signal in Supplementary Fig. S5A (indicated by the black rectangle). The expressing population was sorted to yield a library, designated CT-NBlib, having a size of 10^6 (represented by the blue fluorescence signal in Supplementary Fig. S5A). The CT-NBlib library was then subjected to affinity maturation for binding to Tie1 by using decreasing concentrations of Tie1 for each sorting gate (Supplementary Fig. S5B-F). From the last sort, 20 individual clones conferring the strongest affinity to Tie1 were isolated (Supplementary Fig. S5G). The apparent affinity of each YSD nanobody clone to Tie1 was determined, and the most potent clones were sequenced and cloned into an expression vector. Here again, our attempts to produce these variants as soluble proteins were unsuccessful due to their lack of expression or low stability in *S. cerevisiae*.

Screening a predesigned nanobody library against Tie1 produced a nanobody exhibiting high expression and high affinity for Tie1

In our search for a stable nanobody exhibiting high affinity to Tie1 and high expression, our third approach was based on the naïve, but predesigned, synthetic library that was previously developed by McMahon et al. using a combination of computational and experimental methods (36). In this nanobody library, designated Predes NBlib, positions in the CDR loops had been optimized for expression and

stability of the nanobodies. Predes NBlib was expressed in *S. cerevisiae* using the pYDS649 plasmid (36), with expression of the library (on the cell wall) being detected by targeting the HA-tag expressed at the C-terminus of the nanobody library (Fig. 1B). The Predes NBlib library, with a size of 10^8, was then sorted for Tie1 binding using the same YSD method as that applied for the Naïve NBlib library (Fig. 1A). Following the final (i.e., fifth) round of affinity sorting against Tie 1 as the target, 20 individual nanobody clones were randomly selected and isolated, and the affinity of each clone for soluble Tie1 (25 nM) was determined (Fig. 1C). Nine clones with high binding (normalized to expression) levels were sequenced. Among these clones, the optimal pI value for production – in terms of optimal secretion and low interaction with the yeast membrane during production (40) – i.e., pI 4.96 (Supplementary Table S2), was exhibited by clone NB19. This clone was successfully produced recombinantly in *Pichia pastoris* strain GS115 and purified by affinity chromatography, followed by SEC (Supplementary Fig. S6A, B). The yield was 1 mg/mL of cultured yeast. SDS-PAGE and mass spectrometry (MS) analysis confirmed that NB19 was pure (Fig. S6A, B) and had been produced with the correct molecular weight of 15.7 kDa (Supplementary Fig. S6C).

The purified NB19 nanobody binds Tie1 with high affinity

The selectivity of the binding of NB19 for Tie1 (vs. Tie2) is reflected by the K_D values – calculated from the SPR results – for the binding of immobilized NB19 to Tie1-ECD and Tie2-ECD, namely, 0.170 nM (K_{on} 1.09×10^5 M^1s^{-1}; K_{off} 1.86×10^{-5} $M^{-1}s^{-1}$) and 6 nM (K_{on} 6.85×10^4 $M^{-1}s^{-1}$; K_{off} 4.18×10^{-4} $M^{-1}s^{-1}$), respectively (Fig. 2A, B). The same binding tendency was found for the binding of NB19, at different concentrations, to HEK293 cells transfected with Tie1, Tie2, or both (Fig. 2C), with the K_D values for HEK293 cells overexpressing Tie1 or Tie2 being 0.09 nM and 10 nM, respectively (Fig. 2D). Of note, an excellent fit (R^2 = 0.978) was obtained for a two-phase binding model in HEK293 cells expressing both Tie1 and Tie2, reflecting the differences in affinities for the two receptors. Similarly, affinity titration curves of NB19 binding to glioblastoma U87-MG or human endothelial TIME cells, which endogenously express both Tie1 and Tie2, also showed an excellent fit (R^2 = 0.98 and R^2 = 0.97 for U87-MG or TIME cells, respectively) to a two-phase binding model (Fig. 3). The apparent K_D values of NB19 binding to U87-MG and TIME cells were 1.5 nM and 1.8 nM, respectively. Microscopy experiments confirmed the binding of NB19 to Tie1 and Tie2 (Fig. 2E). As expected, no binding was observed for NB19 to untransfected HEK293.

Tie1-dependent inhibition of the phosphorylation of RTKs in TIME cells

Next, we aimed to test the phosphorylation dependency of Tie2 (and other RTKs) on Tie1, and the effect of NB19 on this axis of RTK activation. For this purpose, we used three specific siRNAs (i.e., 13.1, 13.2 and 13.3) to knock down Tie1 expression in TIME cells (Supplementary Fig. S7). As expected, treatment with siRNA reduced Tie1 expression levels in non-supplemented conditioned medium (Supplementary Fig. S7) and in conditioned medium supplemented with Ang1 (Fig. 4A) compared to the expression levels of the negative control (NC)-siRNA-untreated cells. In support of Tie1/Tie2 cross-talk (4), a significant reduction was also obtained for Tie2 phosphorylation upon silencing Tie1 expression in both untreated

and Ang1-treated cells (Fig. 4B). Furthermore, Ang1-dependent phosphorylation of Akt and FAK, which are downstream of Tie1 in the activation axis, was significantly decreased following the silencing of Tie1 expression (Fig. 4C, D). Of note, similar to the effect of silencing Tie1 expression (by siRNA) on the phosphorylation of RTKs (i.e., Tie2, Akt and FAK), we observed a dose-dependent inhibition of the phosphorylation of those RTKs and of Tie1 upon treatment with NB19 (Fig. 5).

NB19 inhibits tube formation in endothelial cells

To test whether NB19 inhibits Tie1-dependent tube formation, TIME cells were seeded on a layer of pre-solidified Matrigel in a 24-well plate. Following 18 h of incubation with NB19, several parameters of the tube network were quantified using confocal microscopy imaging and computed software analysis (Fig. 6). Treating the cells with 30 nM of NB19 (the concentration at which it binds mostly Tie1) or with 300 nM (the concentration at which it binds both Tie1 and Tie2) led to a decrease in the total tube length and in the number of junctions, in a dose dependent manner, with levels falling below the basal value (Fig. 6B, C). Even at the basal level (without adding external Ang1), endogenous Ang1 caused the formation of tubes, and therefore when the nanobody was added, there was a decrease to below the basal level. Cell aggregation into tube-like structures started immediately after seeding of cells, and defined tube-like structures became visible after 4 h. A real-time experiment showed that inhibition of tube formation by NB19 started as early as 2 h post treatment, namely, at the same time that the tube started to form in the untreated control samples (1–2 h after plating); this inhibition of tube formation in the NB19-treated (but not in the untreated control) cells continued throughout the entire 24-h experiment (movie in Supplementary Material). In addition to its effects on tube formation, NB19 caused a decrease in endothelial cell proliferation—by 20% at a low NB19 concentration (30 nM) and by 50% at a high concentration (300 nM), as determined by the XTT assay (Fig. 6D).

NB19 suppresses cancer cell migration

U87-MG glioblastoma cells were used to test whether NB19 treatment could inhibit the Ang1-stimulated migration of cancer cells. Cell migration was found to be significantly inhibited, with the wound area exhibiting a ~65% cell free area when treated with 30 nM NB19 compared to control (~7% cell free area). This inhibitory effect was dose dependent such that ~80% of the wound area remained cell free upon treatment with 300 nM NB19 (Fig. 7A,B). As shown in Fig. 7A,B, migration of Ang1-stimulated U87-MG cells was reduced by 45% following 24 h of treatment with 30 nM NB19. Furthermore, this difference in migration (40–50% reduction following treatment with NB19) remained constant for all time points tested. For treatment with 300 nM, the NB19 migration distance was reduced by 65% after 24 h of treatment. This finding showed that NB19 reduced the U87-MG cell migration distance in a concentration-dependent manner and that a low concentration of NB19 was sufficient to inhibit most of the migration. For understanding whether the inhibitory effect of NB19 on cell migration was the result of the inhibition of cell migration per se or the result of a decrease in cell viability, we used a proliferation assay, namely, the XTT assay. The results showed a non-significant decrease in U87-MG cell proliferation upon treatment with a low concentration of NB19 (30 nM) and 30% inhibitory effect upon treatment with a high

concentration of NB19 (300 nM). There was no decrease in cell viability below the basal level, but there was a decrease in migration below the basal level, which means that at both concentrations of NB19 (30 and 300 nM) there was an inhibition of cell migration that was not dependent on cell viability.

Discussion

Any study of an orphan receptor, such as Tie1, as a therapeutic target poses experimental challenges in that the lack of cognate ligands complicates the elucidation of its pharmacology, biological functions, and therapeutic potential. This challenge may be overcome by generating high-affinity camelid-derived nanobodies of a size and topography that make them accessible to the orphan target. Since no Tie1 functional epitopes are known, we sought to develop a nanobody that would act as a binder for Tie1, with the choice of a nanobody – rather than a conventional antibody – being dictated not only by the better accessibility of nanobodies but also by the common restriction preventing antibodies, but not nanobodies, from binding conserved epitopes due to immunological tolerance of self-antigens. As conserved epitopes often drive key protein functions, such as the interaction of Tie1 with Tie2 or other effector proteins not yet identified and allosteric communication with such proteins, a rapid method using yeast-based selection scheme enabled by FACS to identify nanobodies that target such sites provides a robust means to interrogate Tie1 function and was thus used in this study.

The screening protocol developed in this study derives from previous studies using nanobody display technologies (e.g., for preparing whole-cell biosensors) that are based on bacterial or yeast cells (41). Once displayed on the surface of bacterial or yeast cells, nanobodies fold into their native and functional structure. Yeast surface display has thus been used for screening nanobody libraries, which is followed by affinity sorting of selected clones by flow-cytometry (36, 42–45). Nevertheless, to date, the above strategies have been tested on immune, animal-derived nanobody libraries, which restricts their use with synthetic libraries. Another inherent problem of previously developed strategies is that, in many cases, there is not a good correlation between the expression and function of the displayed nanobody variant and its expression and function as a purified protein. This latter disadvantage is especially true for universal, non-animal-derived nanobody libraries, i.e., the synthetic naïve libraries that are used when camelids are not available or, as in the case of Tie1, when the protein (i.e., the antigen) may be toxic to the camelid or is difficult to produce (limiting the quantities available for experimentation). In particular, nanobody variants that are selected from non-immune, synthetic library screens suffer from low expression yields and poor stability. To address these limitations, we developed a nanobody library selection platform designed to pinpoint a nanobody variant that would be able to inhibit, with strong potency and specificity, the Tie1 orphan receptor, while exbiting good stabilty.

Our working hypothesis at the start of the study was that stable high-affinity nanobody binders for Tie1 could be produced with high expression by screening Naïve NBlib, a library of clones randomized on their three CDR loops and based on a backbone sequence originating from a clone selected from a camel-derived immune library that had previously undergone stability screens (39). However, although 20 individual clones were randomly selected and isolated from the seventh affinity sort against Tie1-ECD, our

attempts to produce the selected high-affinity Tie1-ECD variants as soluble proteins were unsuccessful due to a lack of expression in yeast—yet another indication of the challenging nature of the task of constructing stable nanobodies.

To overcome the problem of the lack of expression in a yeast-display system, we treated the parental, naïve NBlib library, with proteases as means to select nanobodies that are properly folded and are hence stable towards degradation by proteases. This notion was based on a previous study demonstrating that unfolded protein variants are susceptible to cleavage by proteases, such as trypsin and chymotrypsin, since their exposed hydrophobic surfaces are readily available for digestion (34). The resulting CT-NBlib library (pretreated with chymotrypsin) was affinity maturated for binding to Tie1-ECD to produce individual clones conferring strong affinity to Tie1-ECD. However, here again, as for the Naïve NBlib library, the individual clones were unstable as soluble proteins.

Being unable to produce nanobody variants that were stable and well expressed from the above naïve, randomly mutated libraries, we posited that the way forward would be to use a tailored (predesigned) nanobody library with CDR amino acid compositions that had previously been optimized for high stability and expression. In fact, there are a number of reports of the retrival, from such predesigned nanobody libraries, of potent nanobodies that have been used in a variety of applications (36, 42–44). To addresses the expression and stability challenges associated with our non-immune, naïve library, we used the predesigned library (designated Predes NBlib) developed by McMahon et al. (36). Sorting of this library for high affinity Tie1-ECD binding enabled us to isolate a stable, high expressing nanobody variant (i.e., NB19) that bound Tie1-ECD with a K_D in the subnanomolar range and that showed selectivity for Tie1-ECD over Tie2-ECD.

Having in hand, for the first time, a reagent (i.e., NB19) that binds to both Tie1 and Tie2 but with preferential binding to Tie1 over Tie2 and that strongly inhibits Tie1 enabled us to dissect out the roles of Tie1 and Tie2 in the Tie1-Tie2 signaling axis, especially the cross-talk between Tie1 and Tie2 and its influence on angiogenesis and cancer cell migration and proliferation. Having done so, we can perhaps reconcile studies producing conflicting results and also throw light on the commonly held belief that Tie1 modulation of Tie2 activity (4, 46) is context dependent. For example, one study showed that Ang1 induced the activation of both Tie1 and Tie2 by promoting the formation of a heteromeric Tie1 and Tie2 complex (16). Other studies have indicated that Tie1 is an inhibitor of Tie2 (47, 48), and yet others have reported that Tie1 association with Tie2 is required for Tie2 activation by Ang1 in mice (16, 49) and that phosphorylation of Tie2 is reduced in Tie1-deleted versus control mice (50). In the current study, we also show that inhibition of Tie1 by NB19 reduces Tie2 phosphorylation. We note that a similar inhibitory effect on Tie2 phosphrylation was obtained by inhibiting Tie1 by siRNA knock down.

Our results using NB19 are consistent with previous results and provide additional evidence that Tie1 is capable of activating both FAK and Akt to promote endothelial survival (1, 51): Previous studies have indeed shown that, when activated, Tie1 may then activate Tie2 and other downstream effectors (i.e., FAK/PI3K/Akt pathway), but we show here for the first time that specific inhibition of Tie1 by NB19

results in a reduction both in FAK/PI3K/Akt pathway activation and in endothelial cell survival. Our results in cells also complement previous reports that Tie1 influences the Tie2 signaling pathway and provide supporting evidence for the cross-talk between Ang1, Tie1 and Tie2, i.e., they show that Tie1 is essential for the Tie2 agonistic activity of Ang1 (4).

Our results also demonstrate that NB19 significantly inhibits Tie1 and Tie2 phosphorylation in a dose-dependent manner and thus acts as a functional antagonist towards Tie1, subsequently leading to diminished cancer migration, growth and angiogenesis. By exploiting the ability of NB19 to bind both Tie1 and Tie2, but with preference for Tie1, we were able to analyze the individual roles played by the two potential targets in pathological processes, including endothelial angiogenesis and cancer migration and growth. NB19, at a low concentration (when bound predominantly to Tie1), was shown to inhibit the formation of the tubular structures in TIME endothelial cells, and a stronger inhibitory effect was obtained at elevated NB19 concentrations. At these high concentrations of NB19, when Tie1 binding is at saturation levels, allowing NB19 to bind Tie2 as well, a stronger inhibition on the downstream processes (Akt and FAK phosphorylation, angiogenesis and cancer migration, and growth) was obtained. Further investigation of the complex and dynamic interactions between the Tie receptors and their molecular regulators and specific inhibitors (such as the nanobody developed in this study) will be critical for maximizing the therapeutic potential of these targets and their signaling pathways.

List Of Abbreviations

RTKs, receptor tyrosine kinases; Ang1, angiopoietin-1; FAK, focal adhesion kinase; PI3K, phosphoinositide 3-kinase; Akt, protein kinase B; LECT2, leukocyte cell-derived chemotaxin 2; CDRs, complementarity-determining regions; PDB, protein data bank; FACS, fluorescence activated cell sorting.

Declarations

Ethics approval and consent to participate: Not applicable.

Consent for publication: Not applicable.

Availability of data and materials: All data generated or analyzed during this study are included in this published article [and its supplementary information files].

Competing interests: The authors declare that they have no competing interests.

Funding: This work was supported by the Worldwide Cancer Research (grant number 20-0238), the European Research Council Proof of Concept grant (grant number 875197) and the United States-Israel Binational Science Foundation (grant number 2019303) to N.P.

Authors' contributions: M.M., N.E. and N.P. designed the research; M.M. and N.E. performed the research; M.M., N.E. and N.P. analyzed the data; M.M. and N.P. wrote the paper. All authors edited the manuscript

and approved the final version.

Acknowledgements: We thank Dr. Alon Zilka and Dr. Uzi Hadad for their technical assistance. SPR experiments were performed at the NIBN Proteomics, Cytometry and Microscopy unit. FACS and microscopy experiments were performed at the Ilse Katz Institute for Nanoscale Science & Technology.

References

1. Kontos CD, Cha EH, York JD, Peters KG. The Endothelial Receptor Tyrosine Kinase Tie1 Activates Phosphatidylinositol 3-Kinase and Akt To Inhibit Apoptosis. Mol Cell Biol. 2002;22:1704–13.
2. Ward NL, Dumont DJ. The angiopoietins and Tie2/Tek: adding to the complexity of cardiovascular development. Semin Cell Dev Biol. England; 2002;13:19–27.
3. Yancopoulos GD, Davis S, Gale NW, Rudge JS, Wiegand SJ, Holash J. Vascular-specific growth factors and blood vessel formation. Nature. England; 2000;407:242–8.
4. Leppänen V-M, Saharinen P, Alitalo K. Structural basis of Tie2 activation and Tie2/Tie1 heterodimerization. Proc Natl Acad Sci. National Academy of Sciences; 2017;114:4376–81.
5. Savant S, La Porta S, Budnik A, Busch K, Hu J, Tisch N, et al. The Orphan Receptor Tie1 Controls Angiogenesis and Vascular Remodeling by Differentially Regulating Tie2 in Tip and Stalk Cells. Cell Rep. Cell Press; 2015;12:1761–73.
6. Sato TN, Tozawa Y, Deutsch U, Karen WB, Fujiwara Y, Maureen GM, et al. Distinct roles of the receptor tyrosine kinases Tie-1 and Tie-2 in blood vessel formation. Nature. 1995. page 70–4.
7. Jones N, Voskas D, Master Z, Sarao R, Jones J, Dumont DJ. Rescue of the early vascular defects in Tek/Tie2 null mice reveals an essential survival function. EMBO Rep. 2001;2:438–45.
8. Puri MC, Rossant J, Alitalo K, Bernstein A, Partanen J. The receptor tyrosine kinase TIE is required for integrity and survival of vascular endothelial cells. EMBO J. 1995;14:5884–91.
9. D'Amico G, Korhonen EA, Anisimov A, Zarkada G, Olopainen T, Hägerling R, et al. Tie1 deletion inhibits tumor growth and improves angiopoietin antagonist therapy. J Clin Invest. 2014;124:824–34.
10. Korhonen J, Partanen J, Armstrong E, Vaahtokari A, Elenius K, Jalkanen M, et al. Enhanced expression of the tie receptor tyrosine kinase in endothelial cells during neovascularization. Blood. 1992;80:2548–55.
11. Bouvard C, Segaoula Z, De Arcangelis A, Galy-Fauroux I, Mauge L, Fischer A-M, et al. Tie2-dependent deletion of α6 integrin subunit in mice reduces tumor growth and angiogenesis. Int J Oncol. Greece; 2014;45:2058–64.
12. Saharinen P, Kerkelä K, Ekman N, Marron M, Brindle N, Lee GM, et al. Multiple angiopoietin recombinant proteins activate the Tie1 receptor tyrosine kinase and promote its interaction with Tie2. J Cell Biol. 2005;169:239–43.

13. Fukuhara S, Sako K, Minami T, Noda K, Kim HZ, Kodama T, et al. Differential function of Tie2 at cell-cell contacts and cell-substratum contacts regulated by angiopoietin-1. Nat Cell Biol. England; 2008;10:513–26.
14. Saharinen P, Eklund L, Miettinen J, Wirkkala R, Anisimov A, Winderlich M, et al. Angiopoietins assemble distinct Tie2 signalling complexes in endothelial cell-cell and cell-matrix contacts. Nat Cell Biol. 2008;10:527–37.
15. Macdonald PR, Progias P, Ciani B, Patel S, Mayer U, Steinmetz MO, et al. Structure of the extracellular domain of Tie receptor tyrosine kinases and localization of the angiopoietin-binding epitope. J Biol Chem. ASBMB; 2006;281:28408–14.
16. Korhonen EA, Lampinen A, Giri H, Anisimov A, Kim M, Allen B, et al. Tie1 controls angiopoietin function in vascular remodeling and inflammation. J Clin Invest. 2016;126:3495–510.
17. Jones N, Master Z, Jones J, Bouchard D, Gunji Y, Sasaki H, et al. Identification of Tek/Tie2 binding partners. Binding to a multifunctional docking site mediates cell survival and migration. J Biol Chem. United States; 1999;274:30896–905.
18. Kim I, Kim HG, Moon SO, Chae SW, So JN, Koh KN, et al. Angiopoietin-1 induces endothelial cell sprouting through the activation of focal adhesion kinase and plasmin secretion. Circ Res. United States; 2000;86:952–9.
19. Kim I, Kim HG, So JN, Kim JH, Kwak HJ, Koh GY. Angiopoietin-1 regulates endothelial cell survival through the phosphatidylinositol 3'-Kinase/Akt signal transduction pathway. Circ Res. United States; 2000;86:24–9.
20. Dumont DJ, Yamaguchi TP, Conlon RA, Rossant J, Breitman ML. Tek, a novel tyrosine kinase gene located on mouse chromosome 4, is expressed in endothelial cells and their presumptive precursors. Oncogene. 1992;7:1471–80.
21. Dumont DJ, Gradwohl GJ, Fong GH, Auerbach R, Breitman ML. The endothelial-specific receptor tyrosine kinase, tek, is a member of a new subfamily of receptors. Oncogene. England; 1993;8:1293–301.
22. Partanen J, Dumont DJ. Functions of Tie1 and Tie2 receptor tyrosine kinases in vascular development. Curr Top Microbiol Immunol. Germany; 1999;237:159–72.
23. Sato TN, Qin Y, Kozak CA, Audus KL. Tie-1 and tie-2 define another class of putative receptor tyrosine kinase genes expressed in early embryonic vascular system. Proc Natl Acad Sci U S A. National Academy of Sciences; 1993;90:9355–8.
24. Xu M, Xu H-H, Lin Y, Sun X, Wang L-J, Fang Z-P, et al. LECT2, a Ligand for Tie1, Plays a Crucial Role in Liver Fibrogenesis. Cell. United States; 2019;178:1478-1492.e20.
25. Cho CH, Kammerer RA, Lee HJ, Steinmetz MO, Ryu YS, Lee SH, et al. COMP-Ang1: A designed angiopoietin-1 variant with nonleaky angiogenic activity. Proc Natl Acad Sci U S A. 2004;101:5547–52.
26. Singhal M, Gengenbacher N, La Porta S, Gehrs S, Shi J, Kamiyama M, et al. Preclinical validation of a novel metastasis-inhibiting Tie1 function-blocking antibody. EMBO Mol Med. 2020;12:1–9.

27. Romer T, Leonhardt H, Rothbauer U. Engineering antibodies and proteins for molecular in vivo imaging. Curr Opin Biotechnol. England; 2011;22:882–7.
28. Tajima N, Tezuka K, Tanimoto A, Miyai A, Tanimoto M, Maruhashi J, et al. JTA-009, a fully human antibody against human AILIM/ICOS, ameliorates graft-vs-host reaction in SCID mice grafted with human PBMCs. Exp Hematol. Netherlands; 2008;36:1514–23.
29. McCamish M, Woollett G. Worldwide experience with biosimilar development. MAbs. 2011;3:209–17.
30. Hamers-Casterman C, Atarhouch T, Muyldermans S, Robinson G, Hammers C, Songa EB, et al. Naturally occurring antibodies devoid of light chains. Nature. Nature Publishing Group; 1993;363:446–8.
31. Kijanka M, Dorresteijn B, Oliveira S, Van Bergen En Henegouwen PMP. Nanobody-based cancer therapy of solid tumors. Nanomedicine. 2015;10:161–74.
32. Zavrtanik U, Lukan J, Loris R, Lah J, Hadži S. Structural Basis of Epitope Recognition by Heavy-Chain Camelid Antibodies. J Mol Biol. 2018;430:4369–86.
33. Mitchell LS, Colwell LJ. Analysis of nanobody paratopes reveals greater diversity than classical antibodies. Protein Eng Des Sel. 2018;31:267–75.
34. Moutel S, Bery N, Bernard V, Keller L, Lemesre E, De Marco A, et al. NaLi-H1: A universal synthetic library of humanized nanobodies providing highly functional antibodies and intrabodies. Elife. 2016;5.
35. Muyldermans S. A guide to: generation and design of nanobodies. FEBS J. 2021;288:2084–102.
36. McMahon C, Baier AS, Pascolutti R, Wegrecki M, Zheng S, Ong JX, et al. Yeast surface display platform for rapid discovery of conformationally selective nanobodies. Nat Struct Mol Biol. 2018;25:289–96.
37. Shlamkovich T, Aharon L, Koslawsky D, Einav Y, Papo N. Targeting the Tie2-αvβ3 integrin axis with bi-specific reagents for the inhibition of angiogenesis. BMC Biol. 2018;16:92.
38. Jonkman JEN, Cathcart JA, Xu F, Bartolini ME, Amon JE, Stevens KM, et al. An introduction to the wound healing assay using live-cell microscopy. Cell Adhes \& Migr. Taylor & Francis; 2014;8:440–51.
39. Rosenfeld L, Sananes A, Zur Y, Cohen S, Dhara K, Gelkop S, et al. Nanobodies Targeting Prostate-Specific Membrane Antigen for the Imaging and Therapy of Prostate Cancer. J Med Chem [Internet]. American Chemical Society; 2020;63:7601–15. Available from: https://dx.doi.org/10.1021/acs.jmedchem.0c00418
40. Santos E, Villanueva JR, Sentandreu R. The plasma membrane of Saccharomyces cerevisiae: Isolation and some properties. Biochim Biophys Acta - Biomembr. 1978;508:39–54.
41. Wendel S, Fischer EC, Martínez V, Seppälä S, Nørholm MHH. A nanobody:GFP bacterial platform that enables functional enzyme display and easy quantification of display capacity. Microb Cell Fact [Internet]. 2016;15:71. Available from: http://www.ncbi.nlm.nih.gov/pubmed/27142225

42. Salema V, Fernández LÁ. Escherichia coli surface display for the selection of nanobodies. Microb Biotechnol. 2017;10:1468–84.
43. Roth L, Krah S, Klemm J, Günther R, Toleikis L, Busch M, et al. Isolation of Antigen-Specific VHH Single-Domain Antibodies by Combining Animal Immunization with Yeast Surface Display. Methods Mol Biol. United States; 2020;2070:173–89.
44. Cavallari M. Rapid Antigen and Antibody-Like Molecule Discovery by Staphylococcal Surface Display. Methods Mol Biol. United States; 2020;2070:79–94.
45. Uchański T, Zögg T, Yin J, Yuan D, Wohlkönig A, Fischer B, et al. An improved yeast surface display platform for the screening of nanobody immune libraries. Sci Rep. 2019;9:382.
46. Yuan HT, Venkatesha S, Chan B, Deutsch U, Mammoto T, Sukhatme VP, et al. Activation of the orphan endothelial receptor Tie1 modifies Tie2-mediated intracellular signaling and cell survival. FASEB J. 2007;21:3171–83.
47. Marron MB, Singh H, Tahir TA, Kavumkal J, Kim H-Z, Koh GY, et al. Regulated proteolytic processing of Tie1 modulates ligand responsiveness of the receptor-tyrosine kinase Tie2. J Biol Chem. 2007;282:30509–17.
48. Seegar TCM, Eller B, Tzvetkova-Robev D, Kolev M V., Henderson SC, Nikolov DB, et al. Tie1-Tie2 Interactions Mediate Functional Differences between Angiopoietin Ligands. Mol Cell. Elsevier Ltd; 2010;37:643–55.
49. Kim M, Allen B, Korhonen EA, Nitschké M, Yang HW, Baluk P, et al. Opposing actions of angiopoietin-2 on Tie2 signaling and FOXO1 activation. J Clin Invest. The American Society for Clinical Investigation; 2016;126:3511–25.
50. Savant S, La Porta S, Budnik A, Busch K, Hu J, Tisch N, et al. The Orphan Receptor Tie1 Controls Angiogenesis and Vascular Remodeling by Differentially Regulating Tie2 in Tip and Stalk Cells. Cell Rep. 2015;12:1761–73.
51. Qu X, Zhou B, Scott Baldwin H. Tie1 is required for lymphatic valve and collecting vessel development. Dev Biol. 2015;399:117–28.

Figures

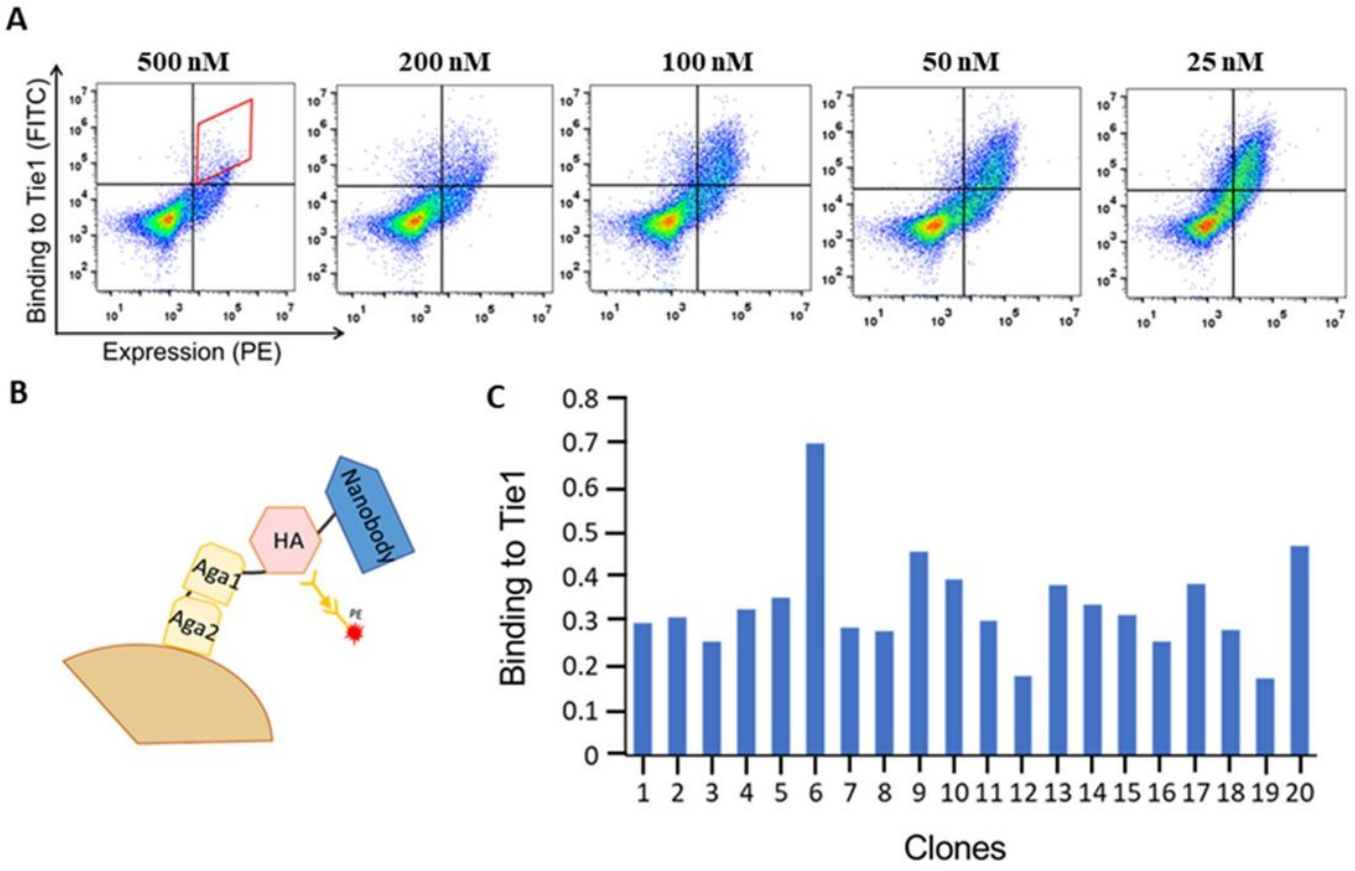

Figure 1

Screening of the computationally designed Predes NBlib library for binding to Tie1. A) Analysis of nanobody library expression and binding to 100 nM Tie1 after sorting against Tie1 at concentrations of 500, 200, 100, 50 and 25 nM (indicated above each panel). The sorting gate for the first sort is shown in red, and gates of the other sorts were identical to the gate shown in A. B) Schematic representation of the Predes NBlib library in the YSD format. C) Binding to Tie1 normalized to expression levels of 20 randomly selected nanobody clones from the fifth sort. The Tie1 binding fluorescence signal for each nanobody clone was divided by its expression signal.

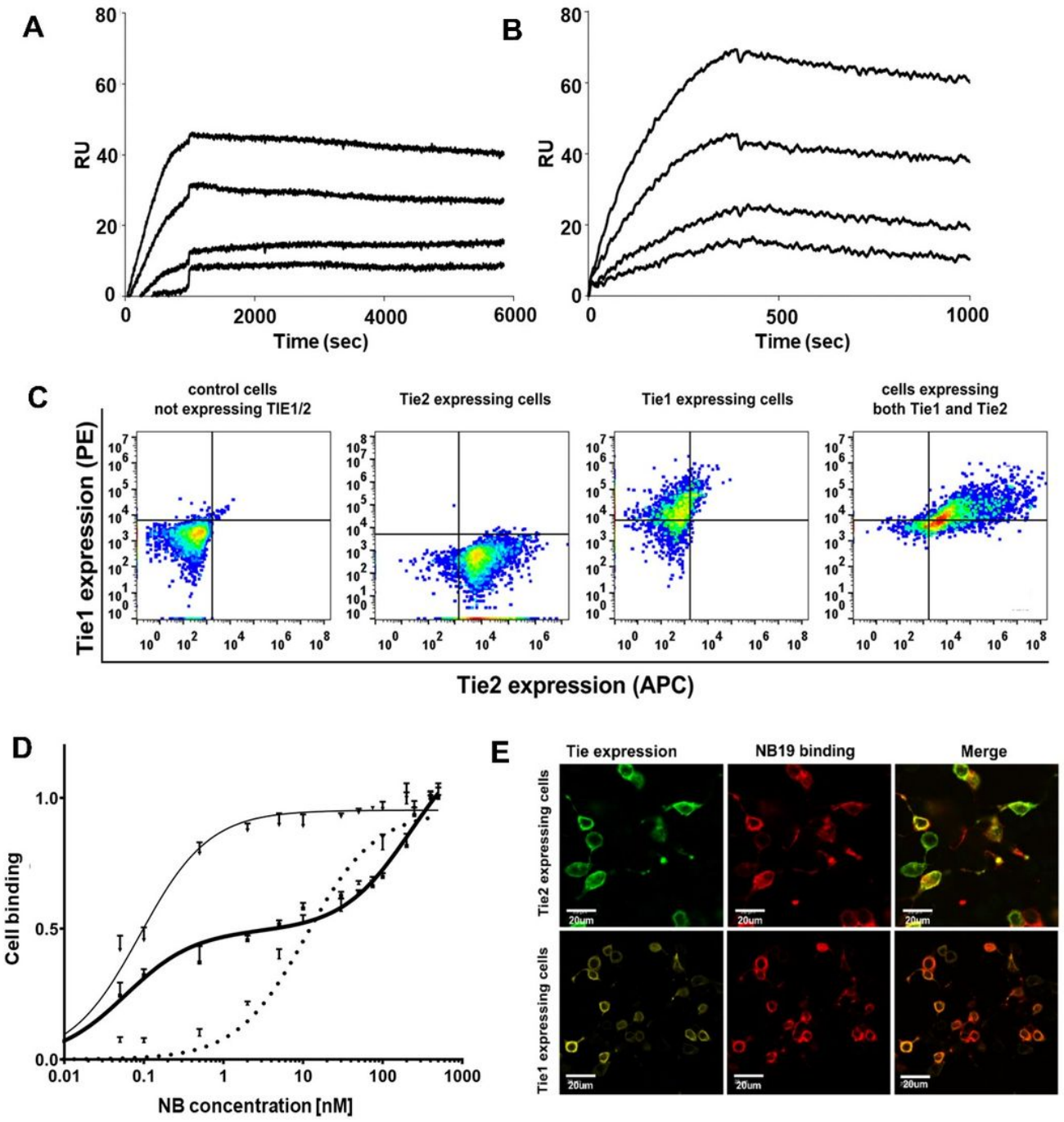

Figure 2

Binding of NB19 to recombinant and overexpressed Tie1 and Tie2. Representative SPR sensorgrams for binding of Tie1-ECD (A) and Tie2-ECD (B) to immobilized NB19. Different concentrations of Tie1-ECD and Tie2-ECD were allowed to flow over immobilized NB19 for 400 s, and dissociation was monitored for 60 min. C) Cell surface expression analysis of Tie2 and Tie1 in transfected vs. untransfected HEK293 cells. HEK293 cells were stained with APC-labeled anti-human Tie2 and PE-labeled anti-human Tie1 antibodies and incubated at 4 °C for 30 min before analysis by flow cytometry. D) Affinity titration curves of NB19

binding to HEK293 cells overexpressing Tie1 (thin black line), Tie2 (dotted black line), or both Tie1 and Tie2 (thick black line). E) Confocal fluorescence microscopy images showing colocalization of NB19 and Tie1 and Tie2 receptors in HEK293 cells overexpressing these receptors. Cell surface expression of Tie2 (green-488) and Tie1 (yellow-PE) are shown; the binding of NB19 was detected by APC anti-his antibody.

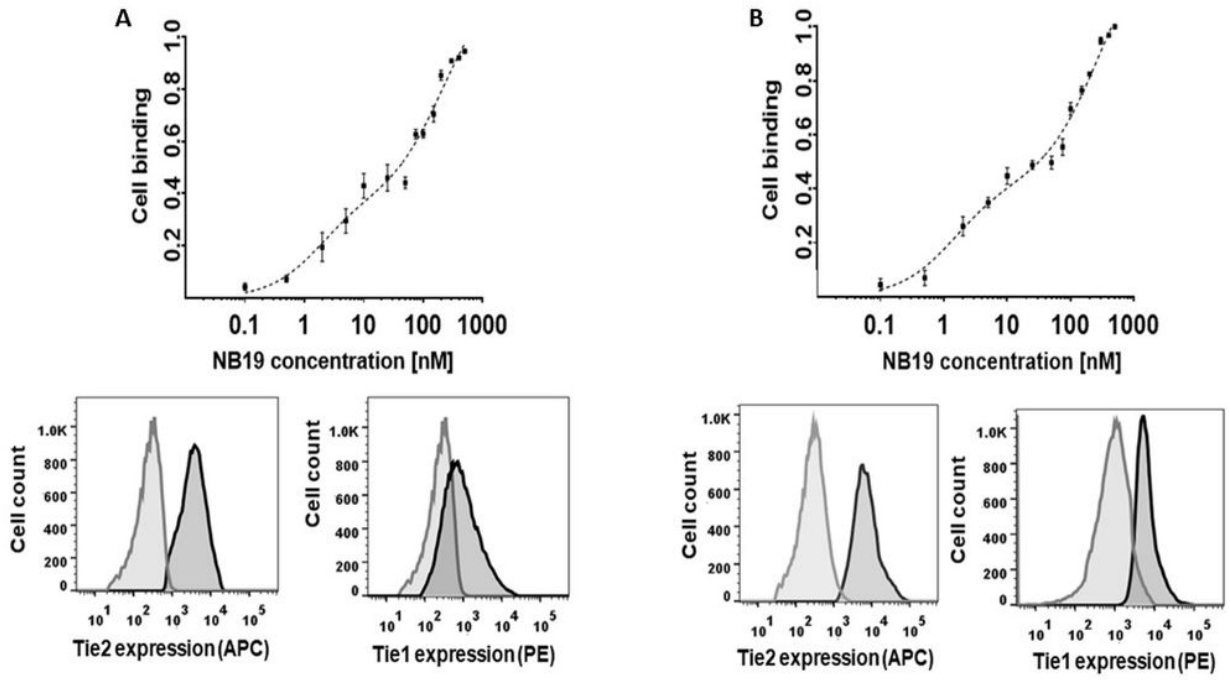

Figure 3

NB19 binding to cells endogenously expressing Tie1 and Tie2. Top panel: Affinity titration curves of NB19 binding to U87-MG cells (A) and TIME cells (B). Two phase binding curves are shown with R^2 = 0.98 and 0.97, respectively. *Bottom panel*: Cell surface expression of Tie2 and Tie1 in stained (dark gray) U87-MG cells (A) and TIME (B) cells is presented in comparison with unstained cells (light gray). In both cases, cells were stained with APC-labeled anti-human Tie2 antibody and PE-labeled anti-human Tie1 antibody and incubated at 4 °C for 30 min before analysis by flow cytometry.

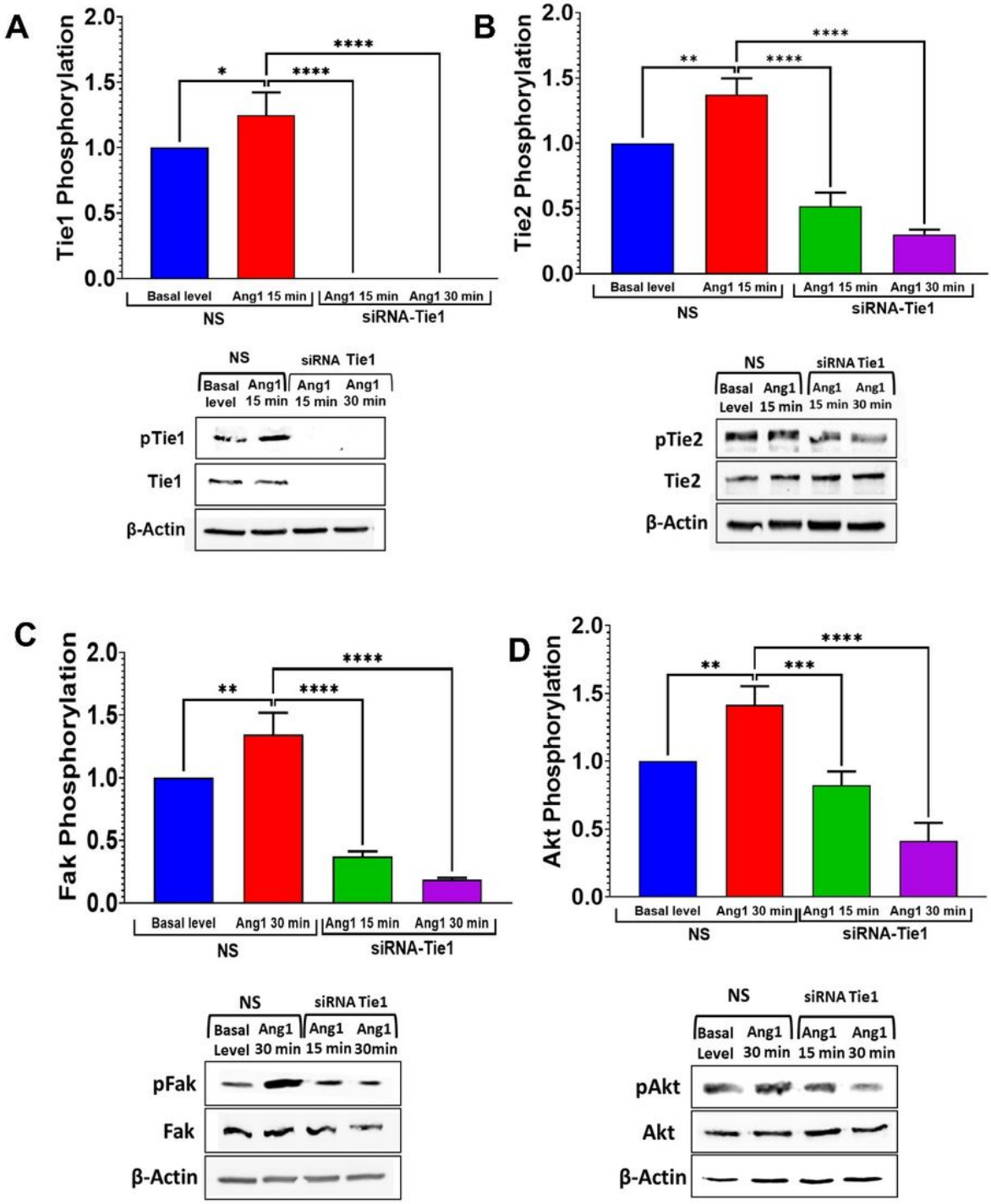

Figure 4

Tie1-dependent inhibition of phosphorylation of RTKs in TIME cells. A) Determination of Tie1 expression and phosphorylation under different conditions: TIME cells were transfected with siRNA-Tie1 or scrambled siRNA (designated NS) and then treated with control buffer (basal level) or 500 ng/mL Ang1 for 15 or 30 min in a 12-well Multidish plate. Cell lysates were analyzed by western blot using antibodies against phosphorylated Tie1 (pTie1), Tie1, and β-actin. B, C and D). Phosphorylation of Tie2, FAK, and

Akt, respectively, was determined as in panel A. In each case, cell lysates were analyzed by western blot using antibodies against the relevant phosphorylated kinase (pTie2, pFAK, or pAkt), the kinase itself (Tie2, FAK, or Akt), or β-actin. The intensity of each phosphorylated band measured by ImageJ software was normalized to the expression of total protein of each experiment, and this value was subsequently normalized to the total quantity of β-actin for each sample. Error bars represent SD. One-way ANOVA with Dunnett's multiple comparison to the Ang1-only treatment was utilized for statistical analysis; *** P < 0.001, ** P < 0.01. NS, non-silenced.

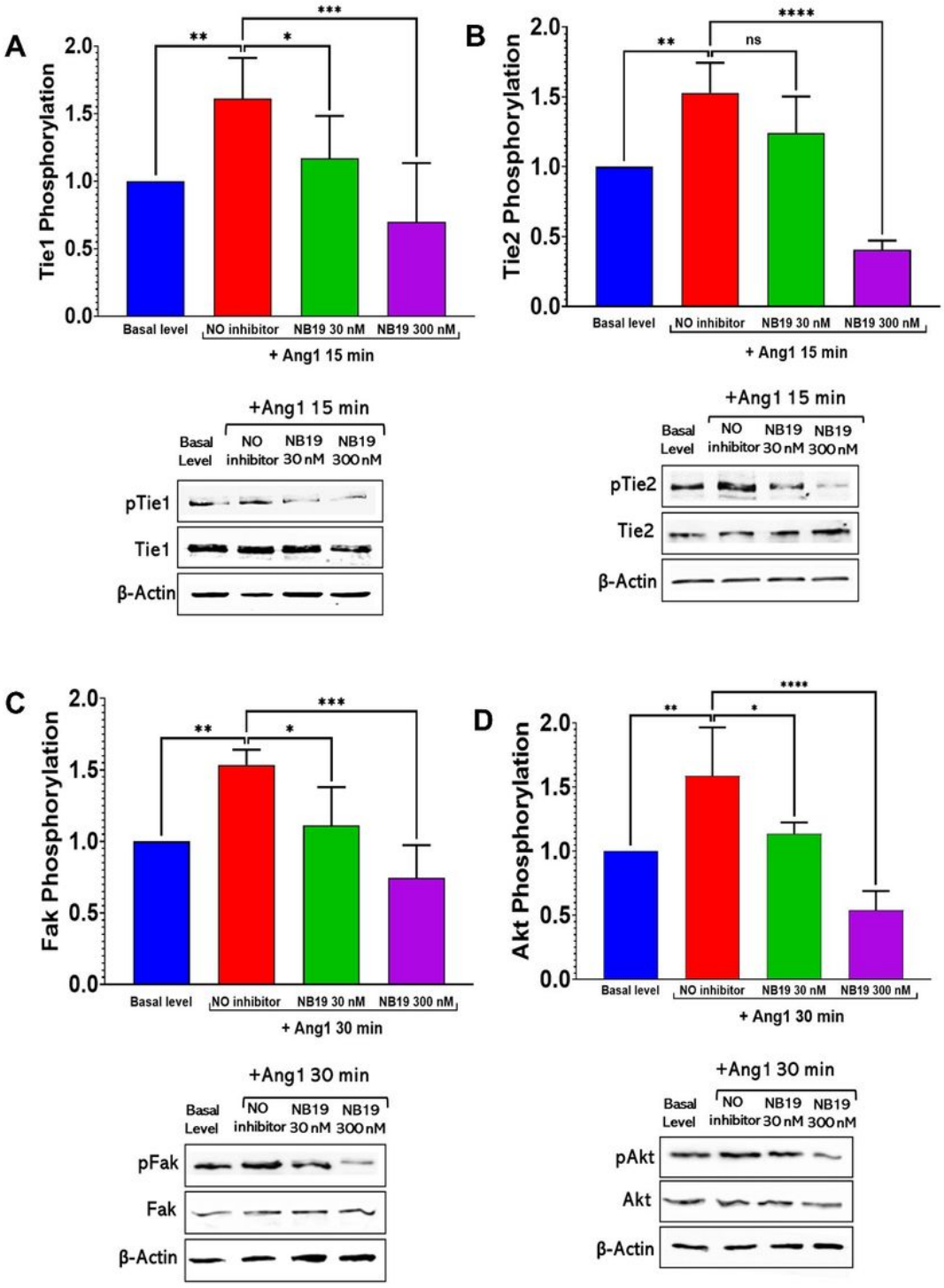

Figure 5

Inhibition of Tie1 and Tie2 phosphorylation by NB19 in TIME cells. A) Determination of Tie1 phosphorylation: TIME cells were treated with buffer (control, basal level), 500 ng/mL Ang1, a combination of 500 ng/mL Ang1 and 30 nM NB19, or a combination of 500 ng/mL Ang1 and 300 nM NB19 for 15 min in a 12-well Multidish plate. Cell lysates were analyzed by western blot using antibodies against phosphorylated Tie1 (pTie1), Tie1 or β-actin. B, C and D) Phosphorylation of Tie2, FAK, and Akt, respectively, was determined as in A, with the exception that the incubation time for Akt was 30 min. Cell lysates were analyzed by western blot using antibodies against the relevant phosphorylated kinase (pTie2, pFAK, or pAkt), the kinase itself (Tie2, FAK, or Akt), or β-actin. The intensities of the phosphorylated bands measured by ImageJ were normalized to the expression levels of total protein in each sample, and this value was subsequently normalized to the total quantity of β-actin for each sample. Error bars represent SD. One-way ANOVA with Dunnett's multiple comparison to the Ang1 treatment was utilized for statistical analysis; *** $P < 0.001$, ** $P < 0.01$. ns, non-significant.

Figure 6

Inhibition of tube formation in endothelial cells by NB19. A) TIME cells were seeded at 1×10^5 in 8-well plates coated with Matrigel and imaged using confocal microscopy following 18 h of treatment under the conditions indicated in the top panels. Scale bar, 100 μm. B, C) Tube structures were analyzed for the number of generated junctions and the total tube length following the different treatments shown on the graphs. * $P < 0.05$; *** $P < 0.001$; **** $P < 0.0001$, n = 3. D) Effects of NB19 on the growth and survival of TIME cells, as reflected in the number of viable cells assessed by an XTT assay. The results for the different samples were normalized to the cell only control. ** $P < 0.01$; *** $P < 0.001$, n = 3.

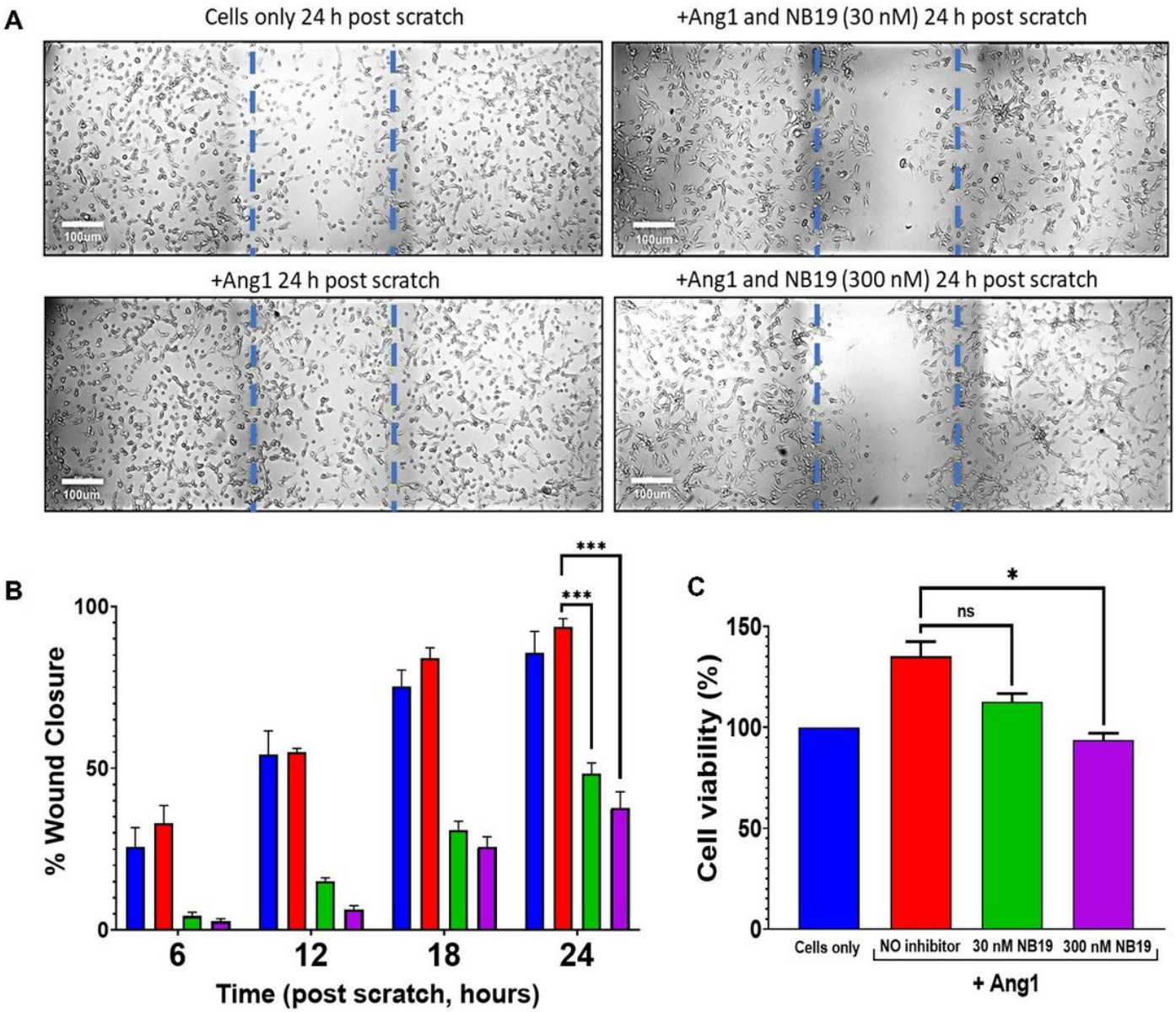

Figure 7

NB19 suppresses cancer cell migration. A scratch assay was performed on U87-MG cells in the presence of 0, 30 or 300 nM NB19. A) Representative photomicrographs of untreated and NB19-treated cells at 24 h post scratch. Broken blue lines indicate the migration front of the cells. B) Summary bar graph illustrating percentage of scratch closure at indicated time points during the assay. The bars are color coded as follows: blue - untreated control cells, red - Ang1-treated cells, green - cells treated with either 30 nM NB19 and Ang1, purple - cells treated with 300 nM NB19 and Ang1. The error bars represent means ± SD of three scratched areas imaged per condition. *** $P < 0.001$. C) Effects of NB19 on the growth and

survival – in terms of % viable cells – of U87-MG cells were assessed by an XTT assay. The results for all samples were normalized to the cells-only control. * $P < 0.05$, ns, non-significant. n = 3.

Supplementary Files

This is a list of supplementary files associated with this preprint. Click to download.

- MayNbpaperSI5.2.22.docx